Acta Crystallographica Section D
Biological Crystallography
ISSN 0907-4449

Rubredoxin from *Clostridium pasteurianum*. Structures of G10A, G43A and G10VG43A mutant proteins. Mutation of conserved glycine 10 to valine causes the 9–10 peptide link to invert

Megan J. Maher,[a] Zhiguang Xiao,[a] Matthew C. J. Wilce,[b] J. Mitchell Guss[b] and Anthony G. Wedd[a]*

[a]School of Chemistry, University of Melbourne, Parkville, Victoria, 3052, Australia, and [b]Department of Biochemistry, University of Sydney, Sydney, NSW, 2006, Australia

Correspondence e-mail: t.wedd@chemistry.unimelb.edu.au

Received 13 November 1998
Accepted 28 January 1999

PDB References: rubredoxin G10A mutant, 1b13; rubredoxin G43A mutant, 1b2j; rubredoxin G10VG43A mutant, 1b20.

The four cysteine ligands which coordinate the Fe atom in the electron-transfer protein rubredoxin lie on loops of the polypeptide which form approximate local twofold symmetry. The cysteine ligands in the protein from *Clostridium pasteurianum* lie at positions 6, 9, 39 and 42. Two glycine residues adjacent to the cysteine ligands at positions 10 and 43 are conserved in all rubredoxins, consistent with the proposal that a β-carbon substituent at these positions would eclipse adjacent peptide carbonyl groups [Adman *et al.* (1975). *Proc. Natl Acad. Sci. USA*, **72**, 4854–4858]. X-ray crystal structures of the three mutant proteins G10A, G43A and G10VG43A are reported. The crystal structures of the single-site mutations are isomorphous with the native protein, space group $R3$; unit-cell parameters are a = 64.3, c = 32.9 Å for G10A and a = 64.4, c = 32.8 Å for G43A. The crystals of the double mutant, G10VG43A, were in space group $P4_32_12$, unit-cell parameters a = 61.9, c = 80.5 Å, with two molecules per asymmetric unit. The observed structural perturbations support the hypothesis that mutation of the conserved glycine residues would introduce strain into the polypeptide. In particular, in the G10VG43A protein substitution of valine at Gly10 causes the 9–10 peptide link to invert, relieving steric interaction between Cys9 O and Val10 C^{β}. This dramatic change in conformation is accompanied by the loss of the 10N—H···O6 hydrogen bond, part of the chelate loop Thr5–Tyr11. The new conformation allows retention of the 11N—H···S9 hydrogen bond, but converts it from a type II to a type I hydrogen bond. This occurs at the cost of a less tightly packed structure. The structural insights allow rationalization of ^{1}H NMR data reported previously for the $^{113}Cd^{II}$-substituted proteins and of the negative shifts observed in the Fe^{III}/Fe^{II} mid-point potentials upon mutation.

1. Introduction

The rubredoxins (Rd) are the simplest of the iron–sulfur proteins, featuring a single $Fe(S\text{-}Cys)_4$ site in a protein of molar mass of approximately 6 kDa (Eaton & Lovenberg, 1973; Holm *et al.*, 1996; Day *et al.*, 1992; Sieker *et al.*, 1994). 14 examples from various anaerobic organisms have been sequenced and five crystal structures have been reported (Day *et al.*, 1992; Sieker *et al.*, 1994; Lee *et al.*, 1995; Mathieu *et al.*, 1992; Dauter *et al.*, 1996). A pseudo-twofold local symmetry is exhibited by the cysteine ligands and the two loops of the protein backbone which carry the cysteine ligands [residues 5–11, 38–44 in the *Clostridium pasteurianum* (Cp) protein; Sieker *et al.*, 1994].

Six N—H···S interactions are features of the site (Fig. 1) forming part of the second coordination sphere which tunes

the reduction potential (Adman *et al.*, 1975; Carter *et al.*, 1974; Stephens *et al.*, 1996; Swartz *et al.*, 1996; Okamura *et al.*, 1998; Denke *et al.*, 1998). A range of 3.25–3.55 Å for N···S distances is consistent with the presence of hydrogen bonds. A number of these distances in the Fe^{III} form of CpRd are outside this range, being termed 'incipient' hydrogen bonds (Adman *et al.*, 1975). These distances are expected to contract upon reduction to Fe^{II} to provide enhanced interactions which will stabilize the increased negative charge at the site (Day *et al.*, 1992).

The S atoms of the interior metal ligands Cys6 and Cys39 each form two hydrogen bonds of types I and III, as classified by Adman *et al.* (1975) by analogy with the N—H···O hydrogen bonds formed in β turns (Adman *et al.*, 1975). Surface metal ligands Cys9 and Cys42 form one hydrogen bond only, of type II. For the latter, it has been suggested that a β carbon on residue 10 or 43 would destabilize such an interaction by eclipsing the carbonyl O atoms of residues 9 or 42, respectively (Adman *et al.*, 1975). Glycine residues are present in equivalent positions in all rubredoxins, consistent with this idea.

Recently, we have probed the effect upon structure and reduction potential of systematic substitution of ligand S atoms for O atoms in the first coordination sphere of CpRd (Xiao *et al.*, 1998). In an attempt to systematically perturb the second coordination sphere, we have isolated mutant Rd proteins in which Gly10 and Gly43 are substituted by alanine and valine, *i.e.* the side-chain H is replaced by CH_3 and $CH(CH_3)_2$, respectively (Ayhan *et al.*, 1996). Changes in physical and chemical properties are consistent with the steric interactions proposed above. The present paper reports X-ray crystallographic analysis of the three mutant proteins G10A, G43A and G10VG43A.

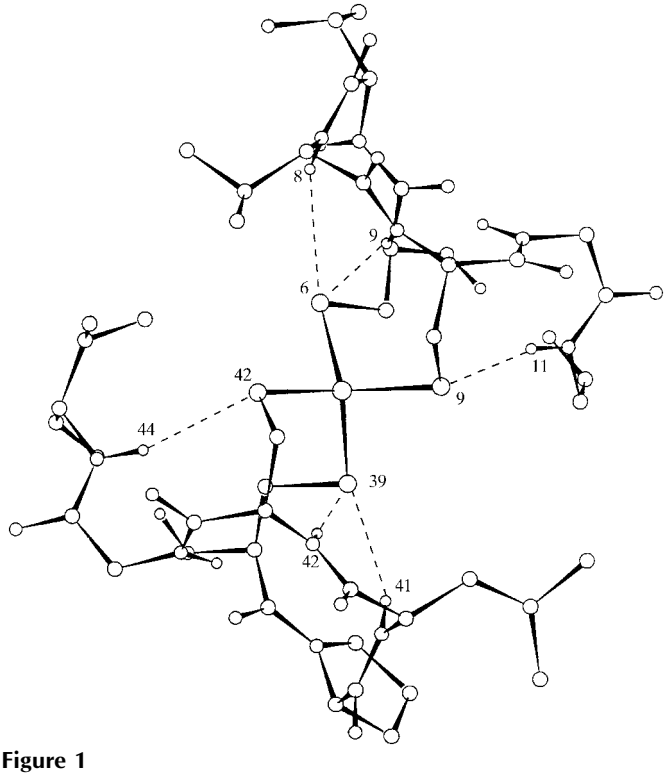

Figure 1
N—H···S interactions (broken lines) around the Fe(S-Cys)$_4$ centre in CpRd (generated from the coordinates of 5rxn in the Protein Data Bank). The pseudo-twofold axis (see text) is perpendicular to the page, passing though the Fe atom.

Table 1
Crystallization conditions.

Protein	$(NH_4)_2SO_4$† (%)	pH	Concentration (mg ml^{-1})
G10A	55	4.0	10
G43A	55	4.5	8
G10VG43A	75	5.0	20

† Concentration in reservoir.

2. Materials and methods

2.1. Crystallization

The recombinant protein rRd and the mutant proteins were generated and purified as detailed previously (Ayhan *et al.*, 1996). Crystals of the proteins were grown under the conditions given in Table 1. Hanging drops containing protein (8 µl, 7–20 mg ml^{-1}), ammonium sulfate (2–35%) and sodium acetate buffer (50 m*M*; pH 4.0–5.0) were equilibrated against a reservoir (700 µl) containing ammonium sulfate (50–70%) in the same buffer. The trays were stored at 277 K and small crystals could usually be observed within 4 d.

2.2. Data collection

Diffraction data were recorded at 293 K on a R-AXIS II imaging-plate detector mounted on a Rigaku RU-200 rotating-anode generator using a 0.2 × 0.2 mm focus. The X-rays (Cu $K\alpha$, λ = 1.5418 Å) were collimated and focused with mirror optics (Molecular Structure Corp.). The data were integrated, scaled and merged using *DENZO* and *SCALEPACK* (Otwinowski & Minor, 1993). A summary of data collection, processing and refinement is given in Table 2.

2.3. Structure solution and refinement

All calculations and manipulations were performed using Indigo XZ Silicon Graphics workstations. The common starting model for refinement and molecular-replacement calculations was the structure of CpRd refined at 1.2 Å resolution (Watenpaugh *et al.*, 1979). Structure calculations were carried out with programs from the *CCP*4 package (Collaborative Computational Project, Number 4, 1994) and *X-PLOR* (Brünger *et al.*, 1987). Initial refinement was carried out with *PROLSQ* or *X-PLOR* (Konnert & Hendrickson, 1980). *REFMAC* was used for the final refinement of all structures (Murshudov *et al.*, 1997). R_{free} validation was based on a subset of 5% of reflections omitted during the entire refinement procedure. Model building and visualization were carried out using *O* (Jones *et al.*, 1991). For all structures, addition of water molecules followed examination of $2F_o - F_c$ and $F_o - F_c$ electron-density maps and the satisfaction of

conservative hydrogen-bonding criteria. The errors in individual atomic coordinates were calculated using the method of Cruickshank (1996) and the estimated standard deviations in calculated bond lengths are quoted in Table 3.

2.4. The G10A and G43A structures

For both structures, refinement was commenced with the 5rxn model from the Protein Data Bank, omitting water molecules. Five cycles of positional and thermal parameter refinement was carried out using *PROLSQ* with data from 7 to 2 Å resolution. The *R* factors were 18.3 and 21.6% for the G10A and G43A structures, respectively. Following this initial refinement, 8σ peaks were observed in the electron-density difference maps within bonding distances of the C^{α} atoms of the mutated residues. The appropriate glycine residue in each case was mutated to alanine and refinement was continued using *REFMAC* (Table 2).

2.5. The G10VG43A structure

Since the space group of the G10VG43A crystals differed from that of native CpRd (Table 2), the structure was solved by molecular replacement using the 5rxn structure (with water molecules omitted) as the search model. The solvent content of the crystals, as given by V_M, the ratio of the volume of the unit cell to the molecular weight of protein in the cell, is 3.14 or 2.10 $Å^3\ Da^{-1}$ for two or three molecules per asymmetric unit, respectively. Both these values are within the normally observed range (Matthews, 1977). The presence of two molecules per asymmetric unit was confirmed by the structure solution. Rotation functions were calculated using all reflections between 8 and 3 Å, with integration radii between 12 and 20 Å, in 0.5 Å steps. The best 40 solutions, using an integration radius of 12.5 Å, were submitted to a translation-function search in each of the enantiomeric space groups, using reflections between 6.5 and 3.5 Å resolution. The top solution, with a correlation coefficient of 0.295, was 46% higher than the next highest peak. The first molecule was then fixed in this position and the remaining rotation-function solutions were subjected to a further translation-function search in order to find the second molecule. The correlation coefficient for the second solution was 0.505, which was 70% higher than the next highest peak. Solutions in space group $P4_32_12$ were clearly better than those in $P4_12_12$ and the choice of the former was confirmed. Electron-density difference maps failed to indicate the presence of a third molecule in the asymmetric unit.

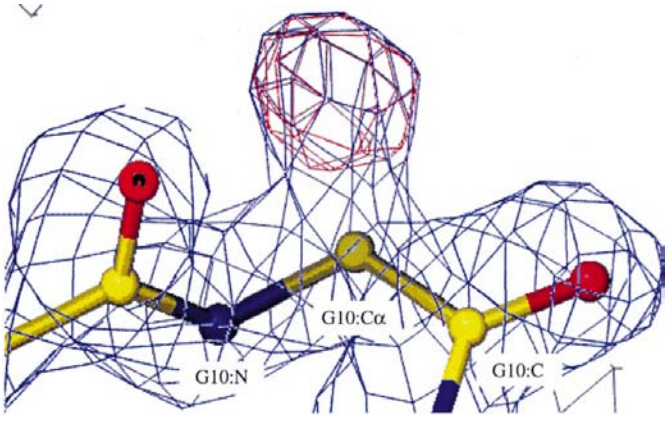

Figure 2
Electron-density difference map of the G10A structure in the vicinity of residue 10. A ball-and-stick model of the Rd structure is colour-coded as follows: carbon, yellow; nitrogen, blue; oxygen, red. The $2F_o - F_c$ electron-density map for G10A is represented in blue. Positive density in the $F_o - F_c$ electron-density map is represented in red. The major positive peak is associated with the Gly10 C^{α} atom, indicating the position of the additional methyl group associated with Ala10.

Table 2
X-ray data.

Figures in parentheses refer to the highest resolution shell.

	G10A	G43A	G10VG43A
Crystal dimensions (mm)	0.3 × 0.3 × 0.2	0.5 × 0.5 × 0.4	0.4 × 0.4 × 0.3
Space group	*R*3	*R*3	$P4_32_12$
a (Å)	64.3	64.4	61.9
c (Å)	32.9	32.8	80.4
Molecules per asymmetric unit	1	1	2
Resolution limit (Å)	1.5	1.6	1.9
Number of observations	29561	17201	54730
Number of unique reflections	7662	6482	12136
Completeness (%)	95 (59)	97 (86)	94 (96)
R_{merge} (*I*)† (%)	8.0 (24.5)	6.7 (21.7)	9.2 (28.0)
R factor‡ (%)	17.1 (38.9)	18.2 (28.2)	19.4 (18.0)
R_{free}§ (%)	19.1 (43.2)	23.4 (36.4)	23.7 (24.5)
Number of solvent waters	40	37	137
Mean *B* factor ($Å^2$)	19	23	27
R.m.s. deviation from ideal values			
Bonds (Å)	0.015	0.016	0.014
Angles (°)	2.0	2.3	2.2
Residues in core regions¶ (%)	93	91	94
Residues in allowed regions¶ (%)	7	9	6

† $R = \sum_{hkl}\sum_{j=1}^{N}|I_o - I_c(j)|/\sum_{hkl}NI_{hkl}$. ‡ $R = \sum_{hkl}||F_o| - k|F_c||/\sum_{hkl}|F_o|$. § Based on a subset of 5% of reflections. ¶ As output from the *PROCHECK* program.

Initial refinement of the model, parameterized as two rigid bodies, was carried out using *X-PLOR* with data in the resolution range 15–4 Å resolution, with corrections for the bulk-solvent contribution to the structure factors. The resulting *R* and R_{free} were 39.5 and 41.5%, respectively. Following two complete cycles of positional and isotropic temperature-factor refinement, the residuals for the model were R = 32.8% and R_{free} = 34.3% for data in the resolution range 50–1.9 Å. The two mutations were evident as positive peaks in electron-density difference maps adjacent to the C^{α} atoms of residues 10 and 43. These electron-density features were present for both molecules in the asymmetric unit. The peak associated with residue 10 was significantly larger in volume than that associated with residue 43 (Fig. 3). Residue 10 was subsequently mutated to valine and residue 43 to alanine in both molecules. Refinement proceeded with the addition of solvent molecules using *REFMAC* (Table 2). Significant features in an electron-density difference map (Fig. 4) near the peptide of residue 10 indicated that the amide group should be flipped.

Table 3
Coordination spheres of the rRd, G10A, G43A and G10VG43A proteins.

Bond distances (Å)

	rRd†	G10A		G43A		G10VG43A		
			Δ‡		Δ‡	§	Av¶	Δ‡
Fe—S6	2.29	2.35	+0.062	2.37	+0.08	2.30, 2.29	2.30	+0.01
Fe—S9	2.25	2.27	+0.02	2.24	−0.01	2.25, 2.23	2.24	−0.01
Fe—S39	2.28	2.29	+0.01	2.32	+0.04	2.34, 2.31	2.33	+0.05
Fe—S42	2.23	2.32	+0.09	2.23	0.00	2.26, 2.24	2.25	+0.02
E.s.d.††	<0.01	0.07	0.08	0.09	0.10	—	0.08	0.09
C^{β}—S6	1.79	1.80	+0.01	1.78	−0.01	1.81, 1.85	1.83	+0.04
C^{β}—S9	1.86	1.83	−0.03	1.84	−0.02	1.83, 1.84	1.84	−0.02
C^{β}—S39	1.81	1.81	+0.00	1.84	+0.03	1.80, 1.80	1.80	−0.01
C^{β}—S42	1.82	1.80	−0.02	1.82	0.00	1.82, 1.80	1.81	−0.01

Bond angles (°)

	rRd†	G10A		G43A		G10VG43A		
			Δ‡		Δ‡	§	Av¶	Δ‡
6S—Fe—S9	113.4	112	−1	112	−1	115, 116	116	+3
6S—Fe—S39	110.1	111	−1	110	0	114, 110	112	+2
6S—Fe—S42	104.3	103	−1	102	−2	104, 104	104	0
9S—Fe—S39	104.6	106	+2	105	0	99, 101	100	−5
9S—Fe—S42	112.7	113	0	116	+3	114, 114	114	+1
39S—Fe—S42	111.9	112	0	113	+1	111, 111	112	0
E.s.d.††	<0.1	2	2	3	3	—	3	3

Dihedral angles (°)

	rRd†	G10A		G43A		G10VG43A§		
			Δ‡		Δ‡	§	Av¶	Δ‡
6C^{α}—C^{β}—S—Fe	169.7	171	+1	172	+2	179, 176	178	+8
9C^{α}—C^{β}—S—Fe	93.8	94	0	97	+3	93, 85	89	−5
39C^{α}—C^{β}—S—Fe	175.8	172	−4	172	−4	179, 178	179	+3
42C^{α}—C^{β}—S—Fe	88.1	92	+4	89	0	87, 91	89	+1
E.s.d.††	<0.1	3	3	3	3	—	3	3

Hydrogen-bond distances (Å)

	rRd†	G10A		G43A		G10VG43A		
			Δ‡		Δ‡	§	Av¶	Δ‡
8N···S6	3.68	3.61	−0.07	3.64	−0.04	3.55, 3.55	3.55	−0.13
9N···S6	3.65	3.58	−0.07	3.63	−0.02	3.66, 3.64	3.65	0.00
11N···S9	3.49	3.48	−0.01	3.47	−0.02	3.45, 3.44	3.45	−0.04
41N···S39	3.54	3.54	0.00	3.51	−0.03	3.61, 3.61	3.61	+0.05
42N···S39	3.58	3.57	−0.01	3.58	0.00	3.55, 3.51	3.53	−0.05
44N···S42	3.84	3.81	+0.03	3.91	+0.07	3.92, 3.89	3.91	+0.07
E.s.d.††	<0.01	0.10	0.11	0.12	0.13	—	0.11	0.12

† From Dauter *et al.* (1996). ‡ Difference between the parameter and that in rRd. § Molecule *A*, molecule *B*. ¶ Average parameter. †† Calculated from the atomic positional error (Cruickshank, 1996).

3. Results

The structure of native CprRd has previously been refined to a very high resolution of 1.1 Å by Dauter *et al.* (1996). This structure can be used as the benchmark for the comparison of the mutant Rd structures in this work. In the native protein, the Fe—S distances to the interior ligands Cys6 and Cys39 are significantly longer than those to the surface ligands Cys9 and Cys42 (Table 3). The S—Fe—S bond angles and C^{α}—C^{β}—S—Fe dihedral angles also reflect tetragonal distortion of the tetrahedral coordination geometry of the active site (Fig. 1).

3.1. The G10A and G43A proteins

All eight Fe—S distances in the G10A and G43A proteins (resolution limits 1.5 and 1.6 Å, respectively) are the same within experimental error (Table 3). However, the pattern of S—Fe—S bond angles (6S—Fe—S42 and 9S—Fe—S39 are more acute than the other four) and C^{α}—C^{β}—S—Fe dihedral angles confirms the retention of the tetragonally distorted iron site (Table 3).

When the structure of rRd is superimposed with those of G10A and G43A, slight perturbations in the orientation of the peptide amide groups in the vicinity of the mutations are observed. These perturbations border on significance, but appear to shift the polypeptide further from the Fe atom: 10NH in G10A and 43NH in G43A both shift by 0.2 (1) Å, relative to their positions in rRd.

Generally, the conformational freedom allowed to proteins *via* rotations about C^{α}—C bonds ensures that C^{β} and carbonyl O atoms are well separated. For example, in the five available Rd structures, Ala $C^{\beta}\cdots O$ distances range from 3.4 to 4.4 Å (estimated from Protein Data Bank files 5rxn, 6rxn, 8rxn, 1rdg and 1caa for the Cp, *Desulfovibrio desulfuricans*, *Desulfovibrio vulgaris*, *Desulfovibrio gigas* and *Pyrococcus furiosus* proteins, respectively). The $C^{\beta}H_3$ groups of the new Ala10 and Ala43 side chains form part of the molecular surfaces of the G10A and G43A proteins (Fig. 2). They might be expected to eclipse O9 and O42, respectively (Adman *et al.*, 1975). The relevant $C^{\beta}\cdots O$ distances are 2.9 (1) and 3.0 (1) Å, much shorter than those previously observed and close to van der Waals contacts (2.8 Å). This is reflected in the backbone torsion angles for Ala10 in G10A and Ala43 in G43A (Table 4). The values for the Gly residues 10 and 43 in rRd lie

in fully allowed regions for glycine but only in the generously allowed regions for alanine in a Ramachandran plot. For the alanine mutants, the respective torsion angles move closer to the allowed values for a left-handed helix in the Ramachandran plot but remain in only the additionally allowed regions. However, the N···S distances characteristic of the N—H···S hydrogen bonds are maintained (Table 3).

3.2. The G10VG43A protein

The geometry around the iron site in both molecules in the asymmetric unit is similar to that seen in the G10A and G43A proteins.

In response to steric interaction between Cys9 O and the Val10 side chain, a major structural change is apparent around position 10 (Fig. 4). Relevant C^{α}—N (φ) and C^{α}—C (ψ) torsion angles are listed in Table 4.

The peptide bond linking residues 9 and 10 has inverted, as indicated by the changes of −162 (6)° in ψ (Cys9) and −176 (6)° in φ (Gly/Val10). The result of the peptide flip is that strain in the polypeptide is relieved and the associated torsion angles for Val10 now lie in a fully allowed region of the Ramachandran plot. The C═O bond of Cys9 now projects inwards towards residues 5–7 of the chelate loop rather than forming part of the molecular surface (Fig. 5). The 10N—H···O6 hydrogen bond, part of the chelate loop Thr5–Tyr11, is lost and replaced by an unfavourable Cys9 O···Cys6 O interaction (2.9 Å) (Fig. 5).

The type II 11N—H···S9 hydrogen bond (Fig. 1) appears to be maintained but has been converted into a type I interaction (Adman *et al.*, 1975); the torsion angles at Cys9 change by −25 (6) and −162 (6)°, respectively. These changes cause the protein chain around Val10 to be displaced away from the Fe atom (Fig. 5). The Val10 side chain is directed into the solvent. The overall structure of the chelate loop and surrounding protein is preserved.

4. Discussion

Within the accuracy of the data (e.s.d's for bond lengths and angles are 0.1 Å and 3°, respectively), mutation of the conserved Gly10 and Gly43 residues of CprRd to alanine and valine does not alter the coordination geometry of the Fe^{III} site (Table 3).

It has been proposed that the presence of glycine residues at positions 10 and 43 is necessary for maintenance of the 11 NH···S9 and 44 NH···S42 hydrogen-bonding interactions (Adman *et al.*, 1975). The stereochemistry necessary to allow the NH functions to achieve a favourable orientation with the ligand S atoms (type II) would lead to β-carbon groups at positions 10 and 43 being eclipsed by Cys9 and Cys42 O groups, respectively. These mutations have not significantly affected the N—H···S hydrogen bonds but have introduced strain into the polypeptide, resulting in the mutant proteins having reduced stability in solution, consistent with this proposal (Ayhan *et al.*, 1996).

For the alanine mutants, there are small changes in the relative orientation of the peptide amide groups around the mutation, leading to a shift of the protein backbone away from the Fe atom: the 10NH function in G10A and the 43NH function of G43A both shift by 0.2 (1) Å relative to their positions in rRd.

Substitution of glycine by valine at Gly10 causes the 9–10 peptide link to invert in the G10VG43A protein, relieving

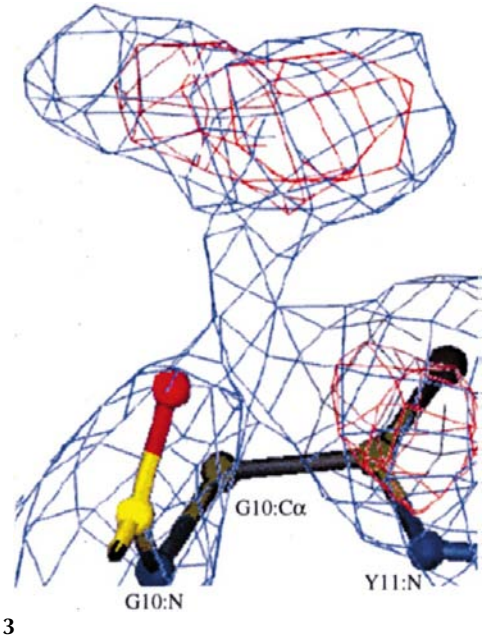

Figure 3
Electron-density difference map for the G10VG434A structure in the region of residue 10. Colour coding as in Fig. 2. Major positive peaks are associated with the Gly10 C^{α} atom, indicating the position of the additional Pr^{i} side chain of Val10.

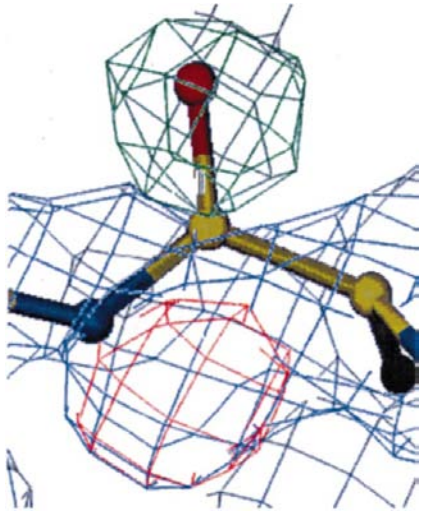

Figure 4
Electron-density difference map for the G10VG434A protein in the region of residue 9. Colour coding as in Fig. 2. Positive and negative electron density in the $F_o - F_c$ map are represented in red and green, respectively. The Cys9 O atom is positioned in an area of negative electron density. A positive peak in the electron-density difference map is present in association with the Cys9 O atom, consistent with inversion of the 9–10 peptide link.

Table 4
Residue torsion angles (φ, ψ; °) of the rRd, G10A, G43A and G10VG43A proteins.

Residue	rRd†	G10A		G43A		G10VG43A		
			Δ‡		Δ‡	§	Av¶	Δ‡
9	−120, −16	−119, −11	+1, +5	−130, −4	−10, +12	−148, −180; −141, −176	−145, −178	−25, −162
10	96, −4	85, 6	−9, +10	89, −3	−7, +1	−80, −12; −80, −4	−80, −8	−176, −4
43	87, 2	79, 7	−8, +5	68, 23	−19, +21	68, 18; 80, 10	76, 14	−11, +12

† From Dauter *et al.* (1996). ‡ Difference between the parameter and that in rRd. § Molecule *A*, molecule *B*. ¶ Average parameter.

steric interaction between Cys9 O and Val10 C^{β} (Figs. 4 and 5). This dramatic change in conformation is accompanied by the loss of the 10N—H···O6 hydrogen bond, part of the structure of the chelate loop Thr5–Tyr11. However, the new conformation allows the 11N—H···S9 interaction to be maintained, although it is converted from a type II to a type I hydrogen bond (Adman *et al.*, 1975).

In the ^{1}H NMR spectrum of the $^{113}Cd^{II}$-substituted G10V protein, large changes in chemical shift (−0.8 to +0.6 p.p.m.) are observed for the NH protons in the Cys6–Tyr11 chelate loop (Ayhan *et al.*, 1996). These were attributed to the $CH(CH_3)_2$ side chain of Val10 occupying part of the surface pocket defined by the CO functions of the loop. It is now apparent that the changes are associated with the altered environments of the NH protons caused by the inversion of the 9–10 peptide bond. On the other hand, small changes (<0.06 p.p.m.) are seen for the NH protons of the Cys39–Val44 chelate loop in the G43V protein, with the single exception of the Val44 NH proton (−0.36 p.p.m.). It is apparent that the 42–43 peptide link has not changed orientation. The 44N—H···S42 interaction involves the only N···S distance sensitive to Cd^{II} substitution (Ayhan *et al.*, 1996).

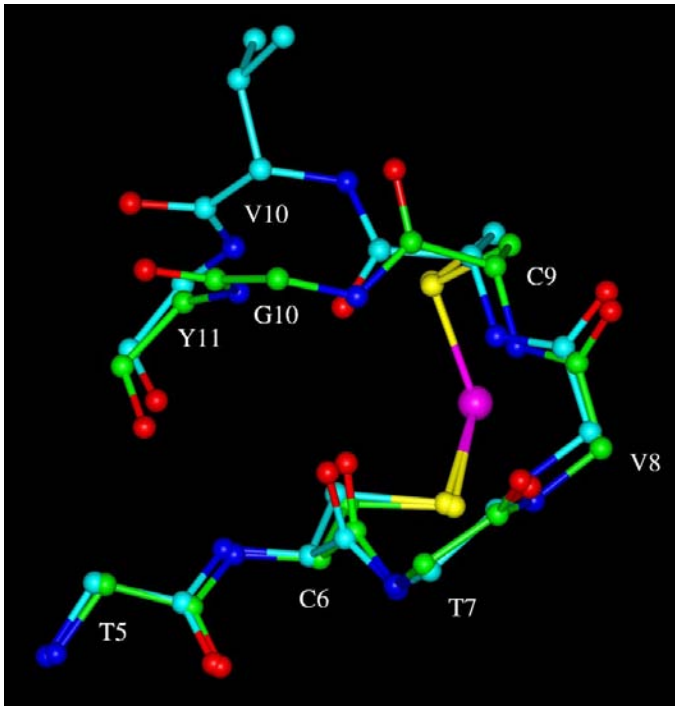

Figure 5
Superposition of the CprRd and G10VG43A protein structures for the the chelate loop 5–11. The C atoms of rRd are represented in green and those of the G10VG43A protein in light blue. The other atoms are represented as follows: nitrogen, dark blue; oxygen, red; sulfur, yellow; iron, pink.

The differential effects of substitution of valine at Gly10 and Gly43, related by the pseudo-twofold symmetry, is emphasized in the double mutant G10VG43V, where the observed chemical shifts correlate closely with those of the single mutants, and also indicate that the effects induced by mutation in one chelate loop are not transmitted to the other. Such localization is consistent with the weak hydrophobic contacts which exist between the chelate loops (Ayhan *et al.*, 1996). The contrasting behaviour appears to be driven by differences in the molecular surface presented by the two chelate loops. The side chains of the residues Thr5 [$CH(OH)CH_3$] and Val38 [$CH(CH_3)_2$] at the start of the Cys6–Tyr11 and Cys39–Val44 loops adopt different orientations (Ayhan *et al.*, 1996).

The proteins with mutations at Gly10 or Gly43 exhibit negative shifts of up to 50 mV in their Fe^{III}/Fe^{II} midpoint potentials relative to that of rRd, implying increased stability of the oxidized [$Fe^{III}(S\text{-}Cys)_4$] centre relative to the reduced form (Ayhan *et al.*, 1996). The effect of incorporation of Val is greater than that of Ala and, in addition, an additivity of the differential effects of the single mutants is seen in double mutants, apparently again owing to the weak interactions only between the chelate loops (*cf* ^{1}H NMR above). The negative shifts can be rationalized by the following interrelated effects, which stabilize the oxidized centres by limiting delocalization of negative charge (Stephens *et al.*, 1996). (i) Perturbations in the orientation of the peptide amide groups in the vicinity of the mutation are observed, which may correlate to a shift away from the Fe atom. In the case of the valine mutation at position 10, the amide group is inverted and orients its negative pole towards the Fe atom. (ii) Substitution of Gly by Ala or Val provides more bulky hydrophobic groups on the protein surface, restricting effective access of solvent water and decreasing the local dielectric constant.

This work was supported by Australian Research Council Grant A29330611 to AGW. MCJW was supported by ARC Grant A29601726 to JMG and Professor H. C. Freeman.

References

Adman, E., Watenpaugh, K. & Jensen, L. H. (1975). *Proc. Natl Acad. Sci. USA*, **72**, 4854–4858.

Ayhan, M., Xiao, Z., Lavery, M. J., Hamer, A. M., Nugent, K. W., Scrofani, S. D. B., Guss, M. & Wedd, A. G. (1996). *Inorg. Chem.* **35**, 5902–5911.
Brünger, A. T., Kuriyan, J. & Karplus, M. (1987). *Science*, **235**, 458–460.
Carter, C. W., Kraut, J. Jr, Freer, S. T. & Alden, R. A. (1974). *J. Biol. Chem.* **249**, 6339–6346.
Collaborative Computational Project, Number 4 (1994). *Acta Cryst.* D**50**, 760–763.
Cruickshank, D. W. C. (1996). *Proceedings of the CCP4 Study Weekend*, edited by E. Dodson, M. Moore, A. Ralph & S. Bailey, pp. 11–22. Warrington: Daresbury Laboratory.
Dauter, Z., Wilson, K. S., Sieker, L. C., Moulis, J.-M. & Meyer, J. (1996). *Proc. Natl Acad. Sci. USA*, **93**, 8836–8840.
Day, M. W., Hsu, B. T., Joshua-Tor, L., Park, J.-B., Zhou, Z. H. , Adams, M. W. W. & Rees, D. C. (1992). *Protein Sci.* **1**, 1494–1507.
Denke, E., Merbitz-Zahradnik, T., Hatzfeld, O. M, Snyder, C. H., Link, T. A. & Trumpower, B. M. (1998). *J. Biol. Chem.* **273**, 9085–9093.
Eaton, W. A. & Lovenberg, W. (1973). *Iron-Sulfur Proteins*, Vol. II, edited by W. Lovenberg, pp. 131–162. New York: Academic Press.
Holm, R. H., Kennepohl, P. & Solomon, E. I. (1996). *Chem. Rev.* **96**, 2239–2314.
Jones, T. A., Zou, J.-Y., Cowan, S. W. & Kjeldgaard, M. (1991). *Acta Cryst.* A**47**, 110–119.
Konnert, J. H. & Hendrickson, W. A. (1980). *Acta Cryst.* A**36**, 344–350.
Lee, W.-Y., Brune, D. C., LoBrutto, R. & Blankenship, R. E. (1995). *Arch. Biochem. Biophys.* **318**, 80–88.
Mathieu, I., Meyer, J. & Moulis, J.-M. (1992). *Biochem. J.* **285**, 255–262.
Matthews, B. W. (1977). *The Proteins*, Vol. III, edited by H. Neurath & R. L. Hill, pp. 468–477. New York: Academic Press.
Murshudov, G. N., Vagin, A. A. & Dodson, E. J. (1997). *Acta Cryst.* D**53**, 240–255.
Okamura, T., Takamizawa, S., Ueyama, N. & Nakamura, A. (1998). *Inorg. Chem.* **37**, 18–28.
Otwinowski, Z. & Minor, W. (1993). *DENZO. A Film Processing Program for Macromolecular Crystallography*. Yale University, New Haven, CT, USA.
Sieker, L. C., Stenkamp, R. E. & LeGall, J. (1994). *Methods Enzymol.* **243**, 203–216.
Stephens, P. J., Jollie, D. R. & Warshel, A. (1996). *Chem. Rev.* **96**, 2491–2513.
Swartz, P. D., Beck, B. W. & Ichiye, T. (1996). *Biophys. J.* **71**, 2958–2969.
Watenpaugh, K. D., Sieker, L. C. & Jensen, L. H. (1979). *J. Mol. Biol.* **131**, 509–522.
Xiao, Z., Lavery, M. J., Ayhan, M., Scrofani, S. D. B., Wilce, M. C. J., Guss, J. M., Tregloan, P. A. T., George, G. N. & Wedd, A. G. (1998). *J. Am. Chem. Soc.* **120**, 4135–4150.